

Supporting Information

Enhancement of optical gain characteristics of quantum dot films by optimization of organic ligands

Sidney T. Malak¹, Evan Lafalce², Jaehan Jung¹, Chun Hao Lin¹,
Marcus J. Smith^{1,3}, Young Jun Yoon,¹ Zhiqun Lin¹, Z. Valy Vardeny², &
Vladimir V. Tsukruk^{1*}

¹School of Materials Science and Engineering,
Georgia Institute of Technology, Atlanta, Georgia 30332, USA

²Department of Physics and Astronomy,
University of Utah, Salt Lake City, Utah 84112, USA

³Aerospace Systems Directorate, Air Force Research Laboratory, Wright-Patterson Air
Force Base, Ohio 45433, United States

Table S1: Table of the optical properties of the QDs before and after the ligand exchange process. A reduction in quantum yield typically occurs after ligand exchange. The reduction in QY is likely due to a decrease in the passivation of surface bonds that can occur when oleic acid is removed and replaced with the amine ligands. The absorbance and emission profiles are similar before and after the ligand exchange procedure.

	Oleic-acid	Hexadecylamine	Octylamine	Butylamine
QY (%)	50	50	20	29
ABS_{1s} (nm)	614	614	617	617
Emission Position (nm)	624	624	624	623
FWHM (nm)	32	34	31	30

Table S2: Table of the predicted stimulated emission lifetime of the ligand-QD films based on the measured refractive index and optical gain values of the QD films. The predicted stimulated emission lifetime was calculated using Eq. S2.

QD-ligand	Predicted Stimulated Build-Up Time (ps)
Oleic acid	94
Hexadecylamine	26
Octadecylamine	12
Butylamine	12

Table S3: Table of the QD-loading (%) of the QD films, the QD volume fraction (%) of the QD solutions (determined by ellipsometry and TGA, respectively), and the thermodynamic properties of each ligand.¹

QD-ligand	Film QD-loading (%)	Solution QD-loading (%)	Solution-Film Difference (%)	Vapor Pressure, 25C (mmHg)	Boiling Point (°C)
Oleic acid	29	27	2	0	360
HDA	34	31	3	0	330
OctA	45	30	15	0.9	175
BA	49	33	16	82	78

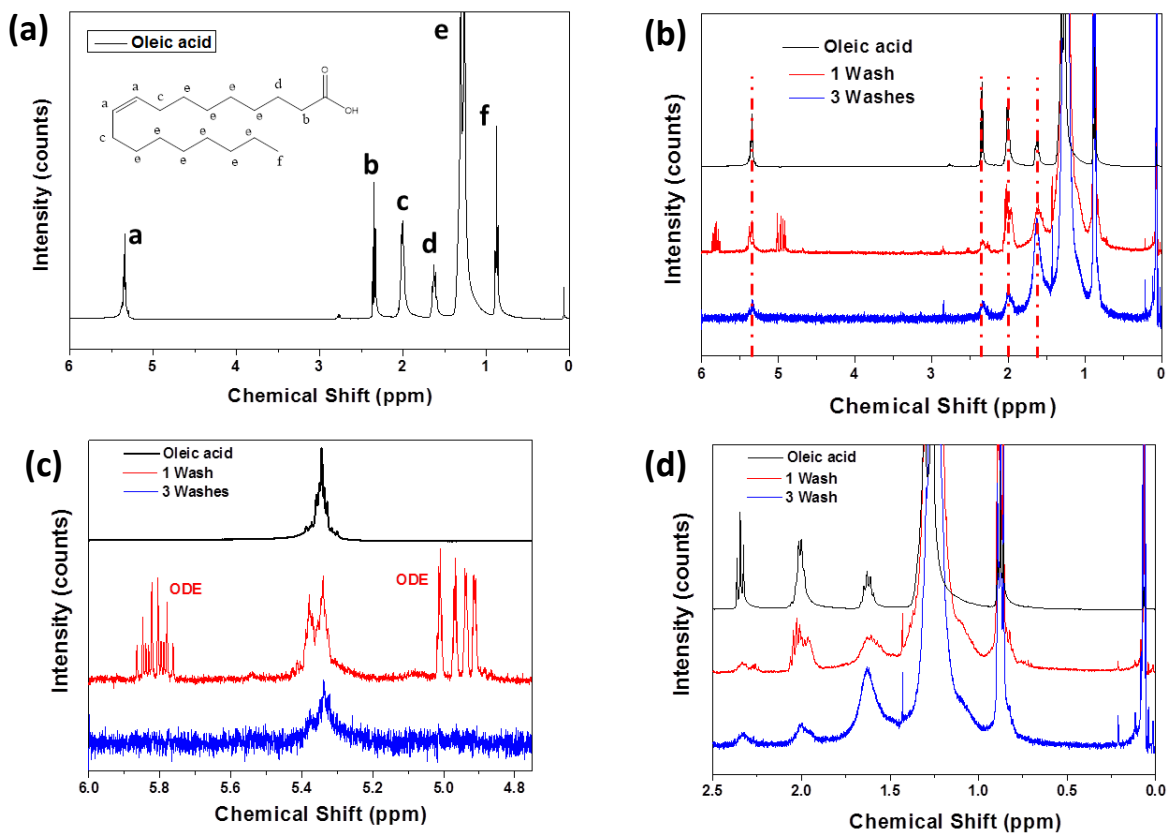


Figure S1: NMR was used to evaluate the effect of washing the ODE/oleic acid capped QDs before the ligand exchange. (a) NMR of oleic acid. (b) NMR of oleic acid capped QDs at different points during the washing process. Examination of the 4.7-6 ppm regions shows (c) that the ODE peaks disappear and that the peak near 5.35 ppm assigned to vinylic hydrogens broadens, indicating removal of excess free oleic acid. (d) Close-up of the 2.5-0 ppm region shows broadening of the 1.6, 2.0, and 2.3 ppm peaks after successive washing.

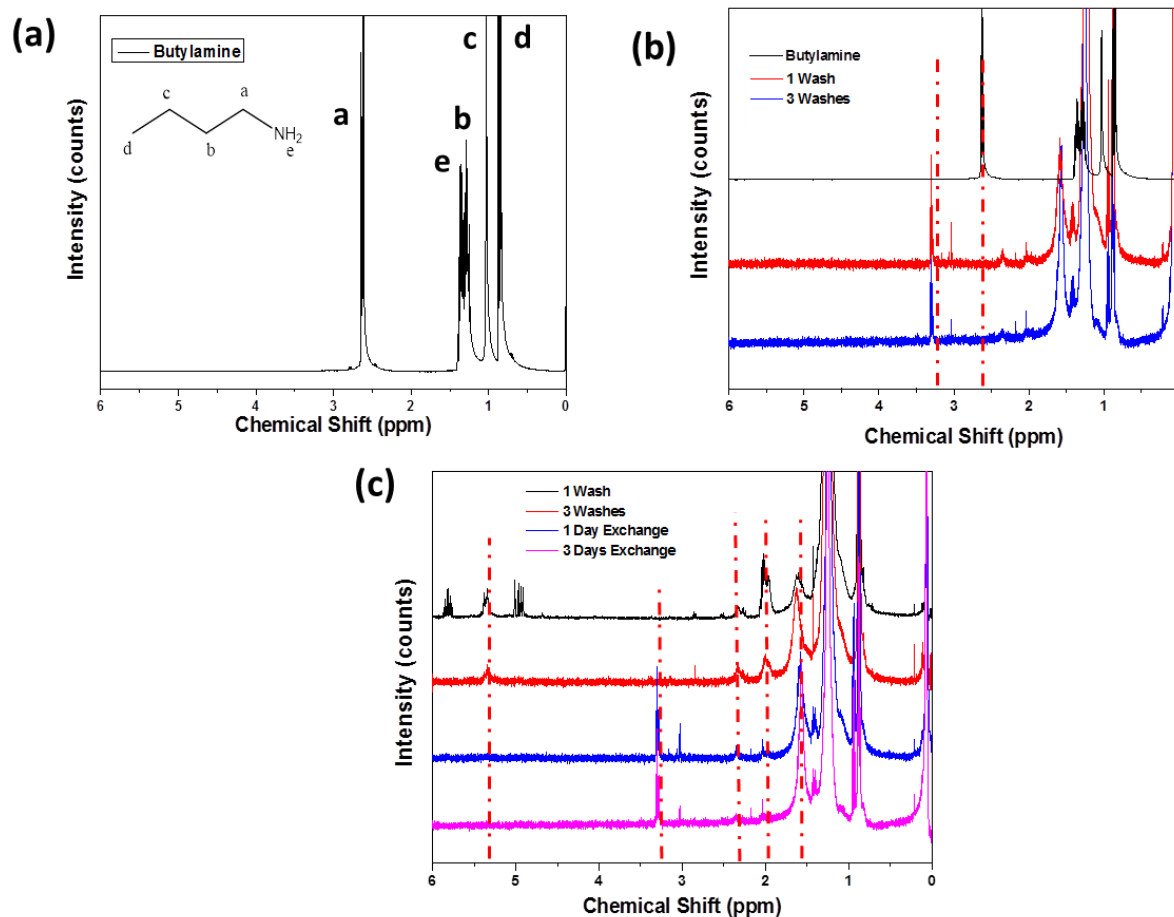


Figure S2: NMR was used to evaluate the efficiency of the ligand exchange. (a) NMR of butylamine (the ligand that will be displacing oleic acid on the QD surface). (b) NMR of butylamine and of QDs that underwent a ligand exchange from oleic acid to butylamine. The BA peak at 2.8 ppm (hydrogen peak) shifts to 3.2 ppm which is likely due to interaction with QD surface. (c) Comparison of NMR from different points in the washing process and ligand exchange process.

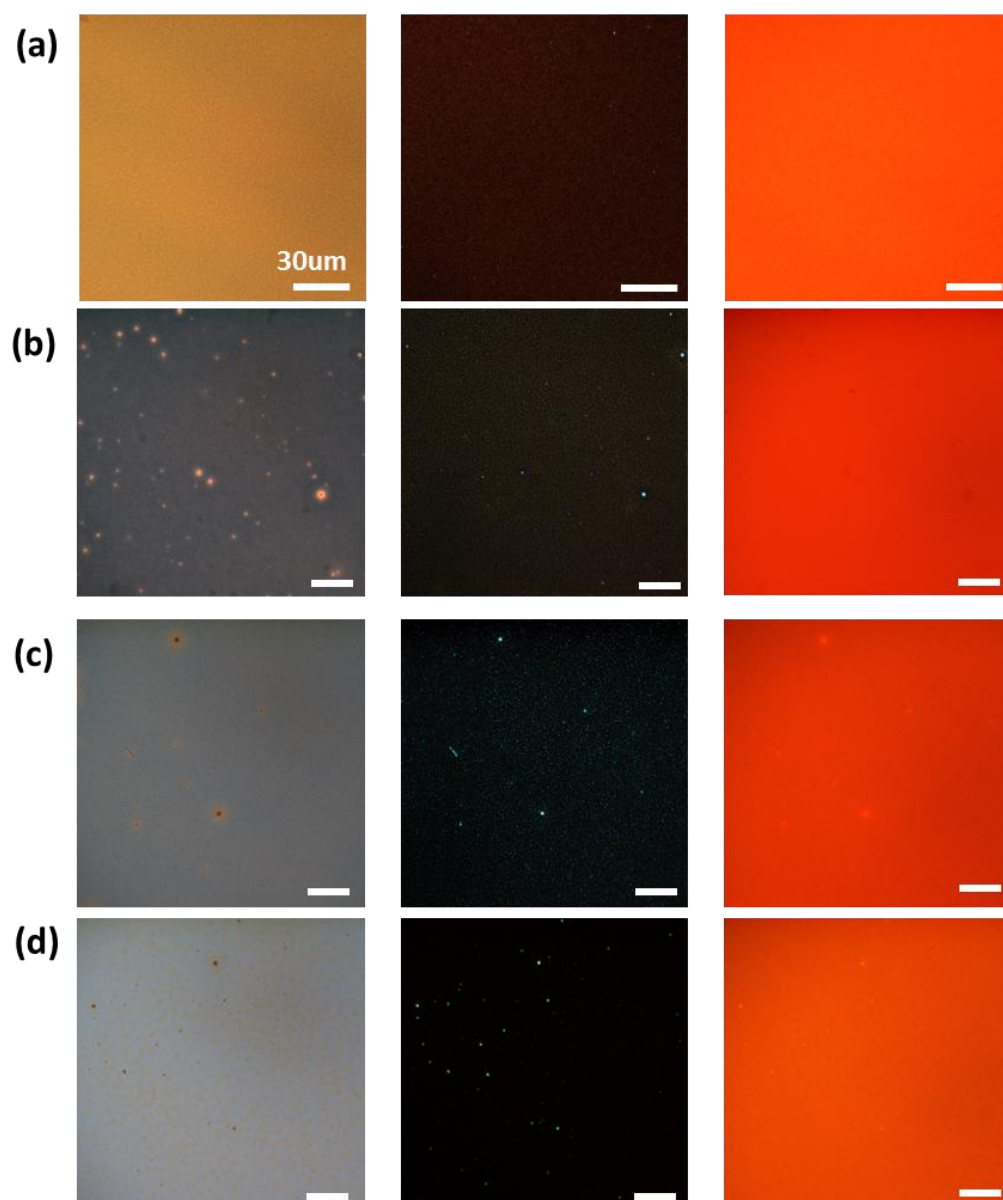


Figure S3: Bright field (column 1), dark field (column 2), and fluorescence (column 3) images of (a) oleic acid, (b) hexadecylamine, (c) octylamine, and (d) butylamine capped QD films. Imaging shows that the films exhibit similar uniform morphology and fluorescence emission as well as some scattering due to surface defects. All scale bars are 30 μm .

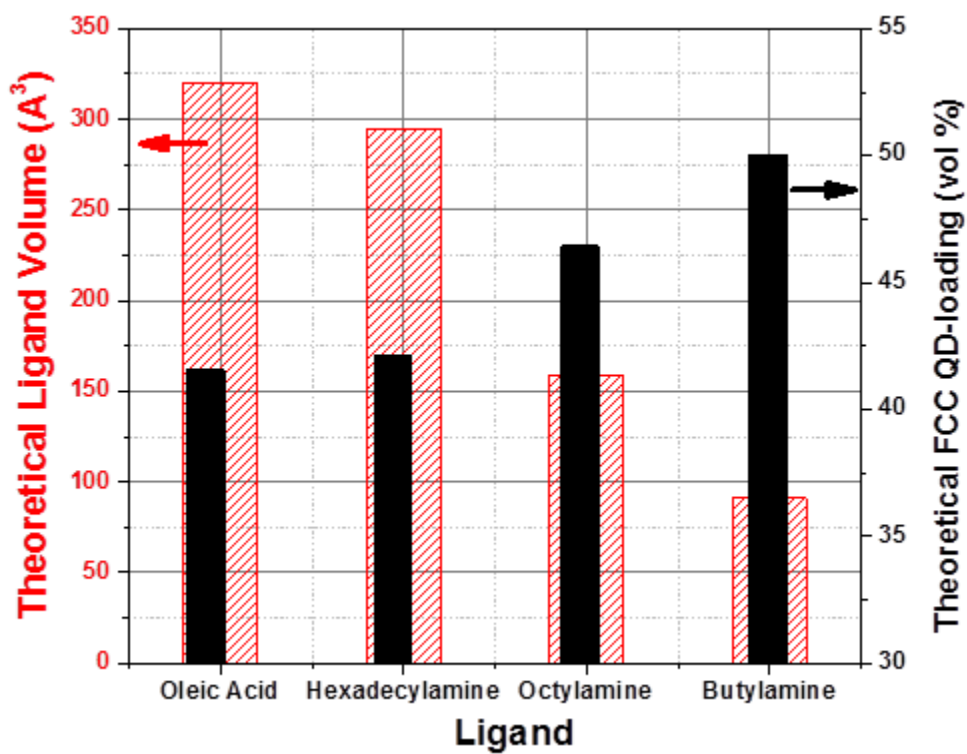


Figure S4: Plot of the predicted free volume of each QD ligand and the corresponding maximum theoretical FCC QD-packing density (assuming diameter of 8 nm). Reducing the size of the ligand leads to a larger maximum FCC packing for the QDs in the film (and vice versa).

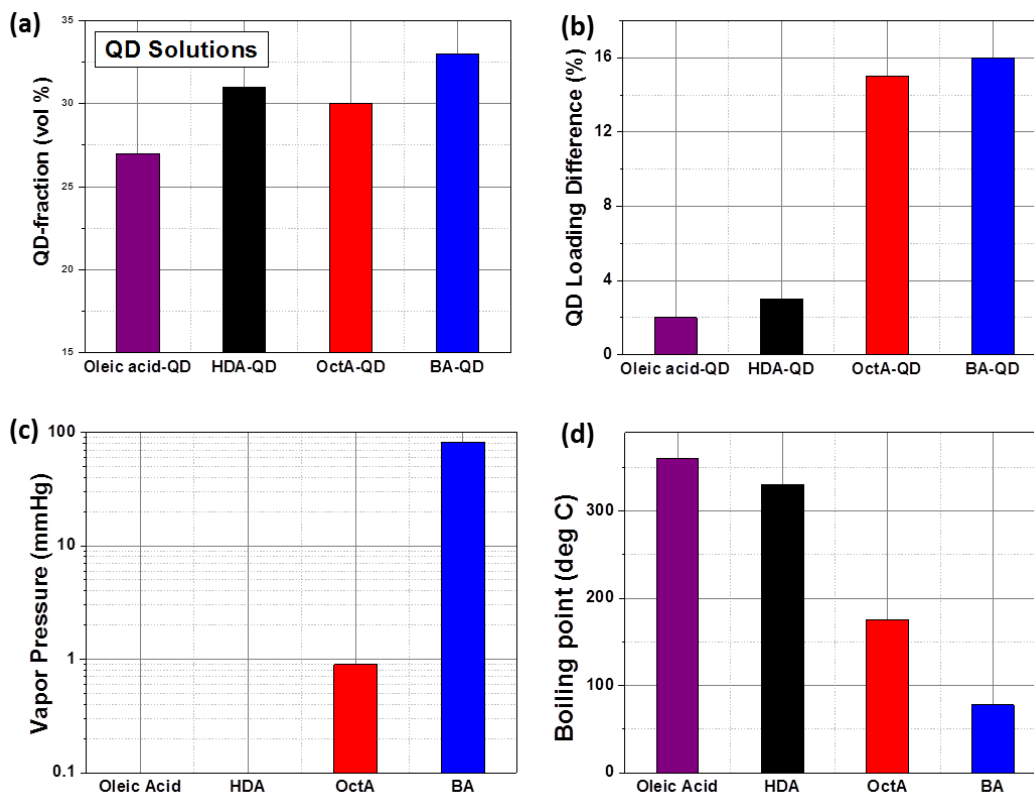


Figure S5: Examination of the QD fraction in solutions and how it compares to QD films. (a) Thermogravimetric analysis (TGA) of QD solutions. (b) The difference in QD volume fraction between QD films and the QD solutions. The (c) vapor pressure and (d) boiling point of each ligand. Note, the vapor pressure of oleic acid and hexadecylamine area very low at room temperature (< 1 mmHg) and therefore were approximated to have a zero value.

There appears to be a difference of QD volume fraction between the QD films and QD solutions. The magnitude of this difference correlates with the volatility of the specific ligand. For example, butylamine-QDs, which display the largest difference between the film state ($49 \pm 6\%$) and solution state (33%) also is the most volatile ligand (highest vapor pressure, lowest boiling point). Note, value ranges are one standard deviation in the film state ($29 \pm 6\%$) and solution state (27%) is the least volatile (lowest vapor pressure (V_p), highest boiling point). This trend occurs for all ligands examined (**Table S3**).

The volatility of the ligand is an important factor affecting the formation of the film during spin-casting and storage. The volatility of the QD ligand has been shown to strongly impact ligand desorption, with a highly volatile ligand (pyridine, $V_p = 20$ mmHg at 25°C) showing large desorption ($\approx 70\%$) under ambient conditions while a low volatility ligand (trioctylphosphine oxide, $V_p \approx 0$ mmHg at 25°C) shows nearly no desorption.^{1,2,3} Therefore, the high volatility of butylamine and octylamine leads to some degree of desorption from the film during storage. Even more importantly, the volatile ligands will experience strong desorption from the film surface during spin-casting (unbound ligands in particular) due to the highly turbulent atmosphere above the film. These two factors thus increase the QD volume fraction and lead to a large difference between the QD volume fraction measured in the film state and solution state.

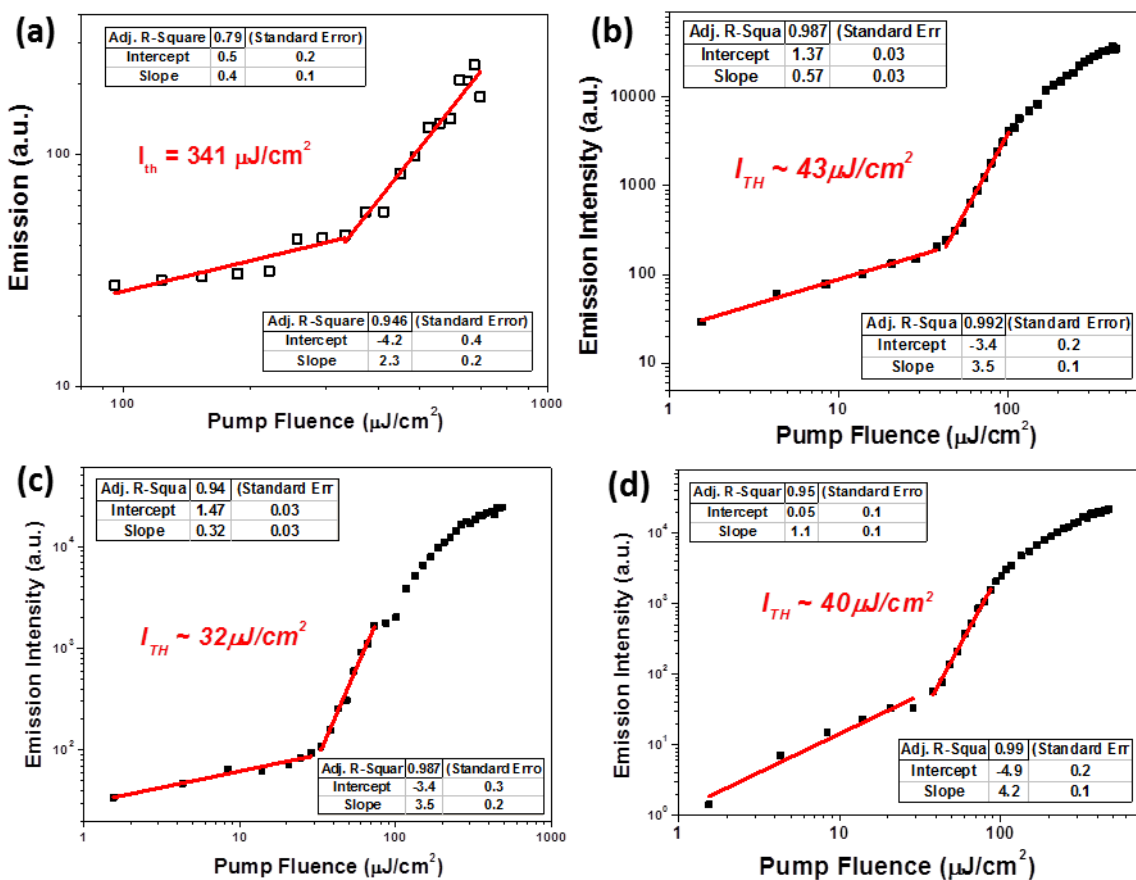


Figure S6: ASE threshold plots and fitting for different QD-ligand combinations. The threshold value of the QD film is determined by linear fitting of the shallow and steep pump fluence versus emission curve. The pump fluence value at the intersection of the linear fit from the two regions is the threshold fluence. Examples of threshold determination are shown for (a) oleic acid-QD, (b) HDA-QD, (c) OctA-QD, and (d) BA-QD films.

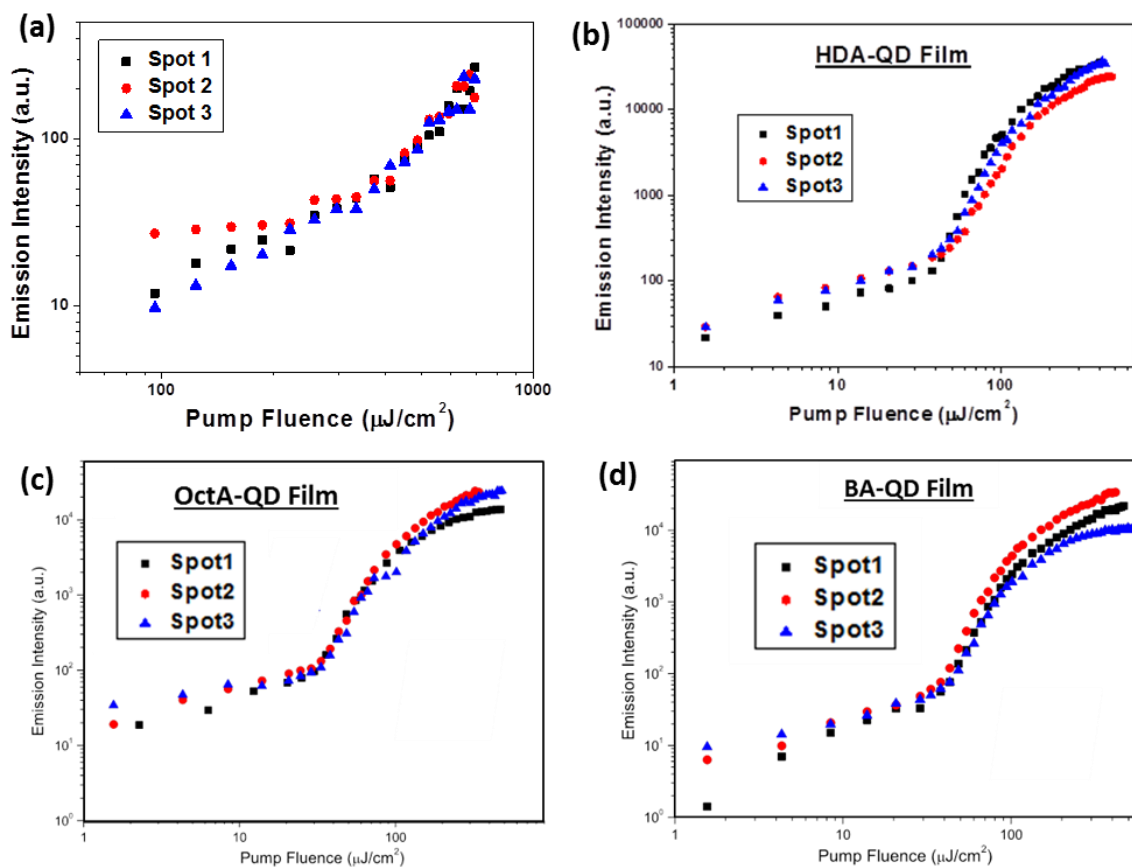


Figure S7: ASE threshold plots for different QD-ligand combinations from multiple spots. The threshold behavior of the QD films was determined by examining how the pump fluence affects the emission intensity. A transition from a shallow slope to a steep slope indicates an ASE threshold. The threshold behavior for each type of QD film was verified over multiple trials. Examples of threshold examination are shown for (a) oleic acid-QD, (b) HDA-QD, (c) OctA-QD, and (d) BA-QD films.

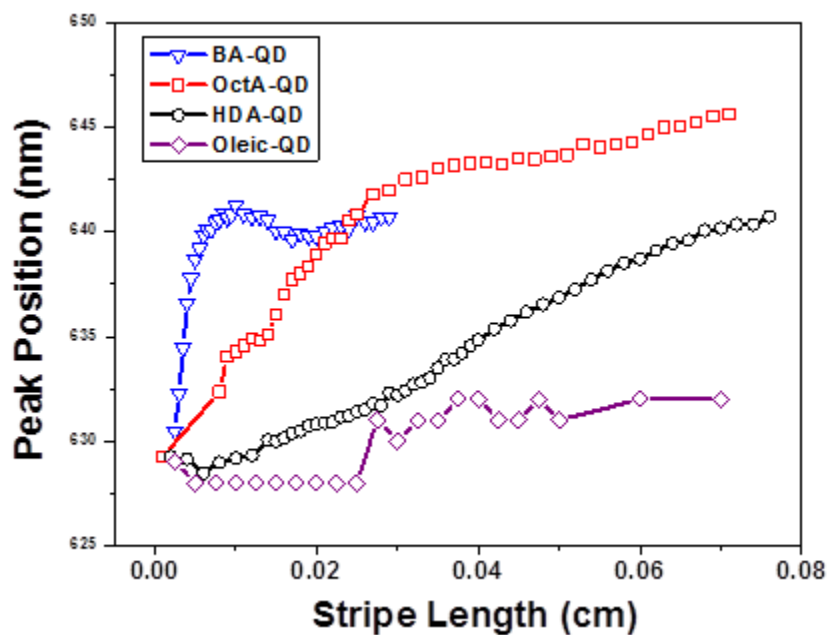


Figure S8: Peak position of the maximum emission peak versus pump strip length. The presence of ASE is supported by examining a number of parameters including a shift of the ASE peak with respect to the PL peak. Typically the ASE peak red-shifts compared to the PL peak due to reabsorption of the emitted light by the film.⁴ All the QD films with amine functionalization in this study exhibited a red-shift of approximately 10-15 nm compared to the PL peak, while the oleic-QD film show a red-shift of only 4 nm, indicating a smaller amount of reabsorption during light propagation.

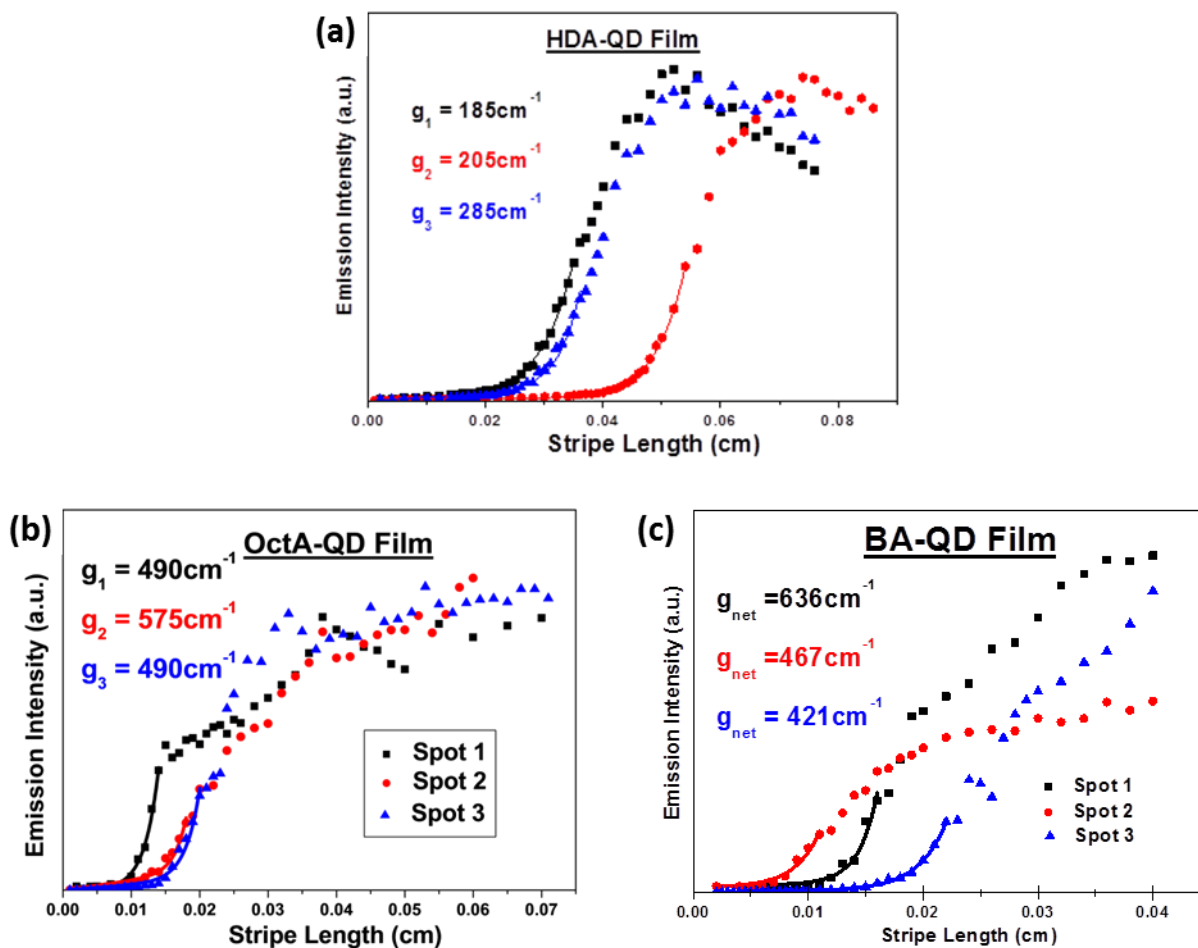


Figure S9: Data of the emission intensity versus pump stripe length from the variable stripe length (VSL) method for various QD-ligand combinations. The optical gain of the QD films was determined by fitting data from the VSL method with an exponential function. The gain value for each type of QD film was determined by averaging over multiple trials. Examples of VSL data and fitting are shown for (a) HDA-QD, (b) OctA-QD, and (c) BA-QD films.

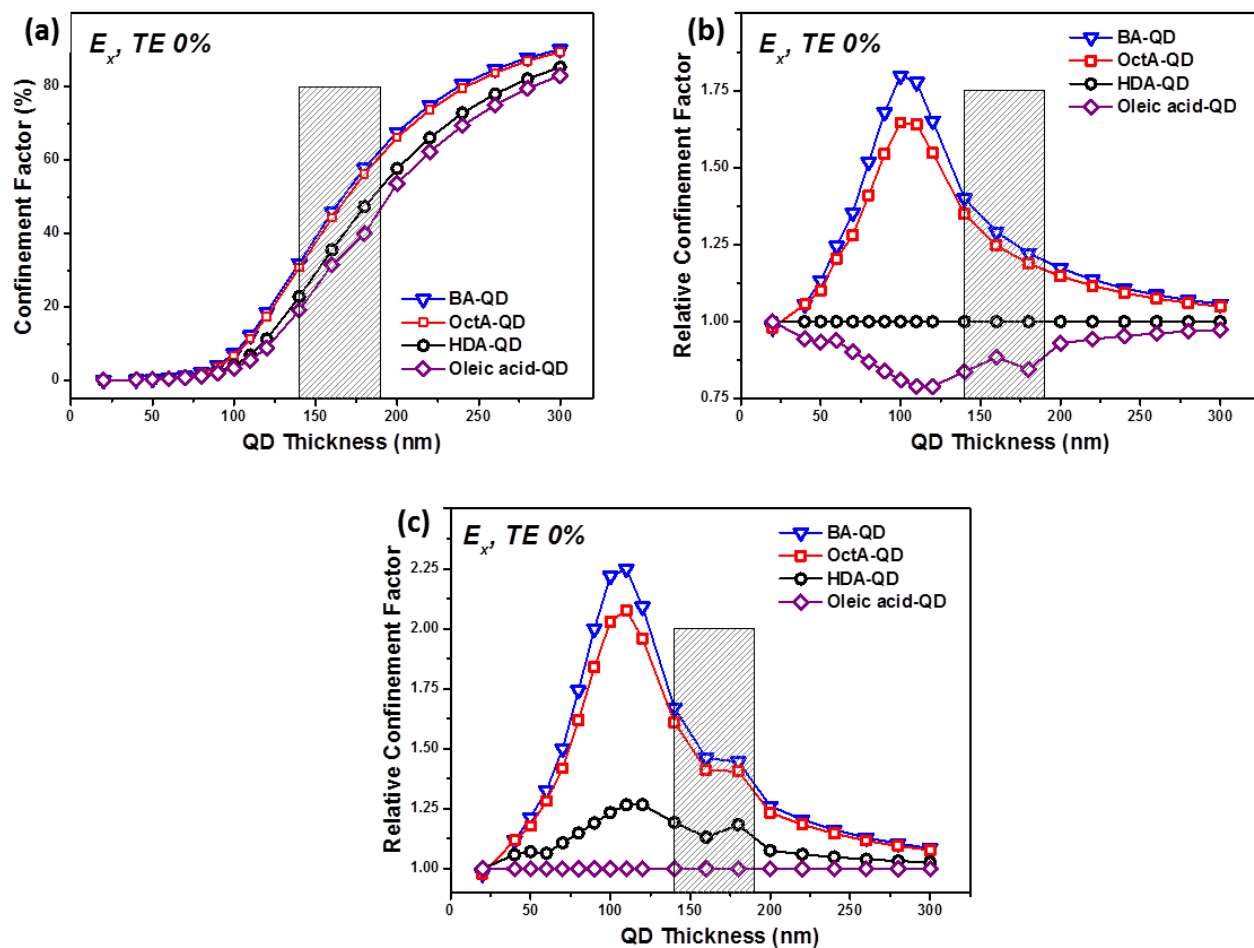


Figure S10: (a) Plot of the confinement factor (E_x , TE 0% mode) at 635 nm for films of different thickness and different refractive index. The relative confinement factor of each film compared to (b) the HDA-QD film and compared to (c) the oleic-QD film. The confinement factor is higher (for a given film thickness) for films with a higher refractive index. The grey shaded areas represent typical QD film thicknesses in this study.

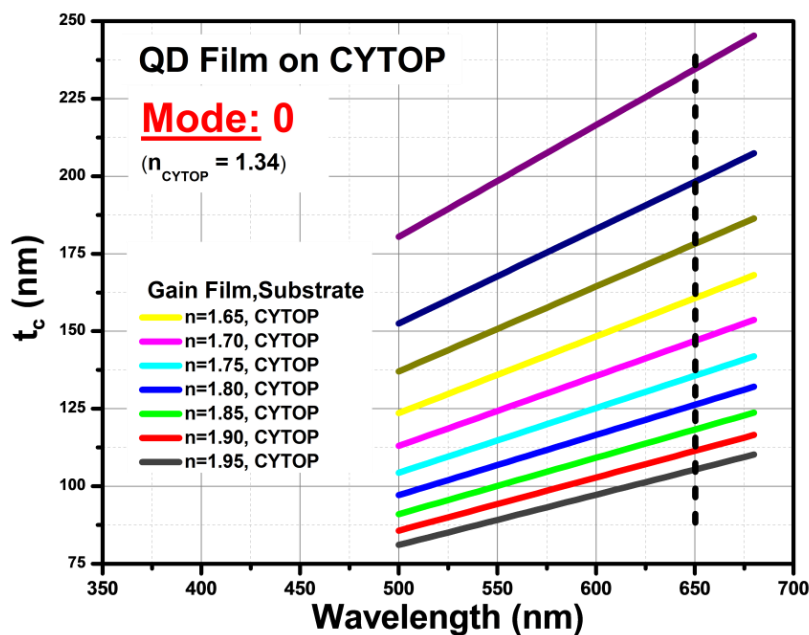


Figure S11: Plot of the critical thickness for the primary waveguiding mode for QD films with different refractive index on a CYTOP film (refractive index of 1.34). The critical thickness indicates the minimum thickness a film requires in order to support at least one waveguide mode. The function used to calculate the critical film thickness (t_c) assumes that the top layer is air.⁵ Each film has a thickness that allows for only one waveguide mode.

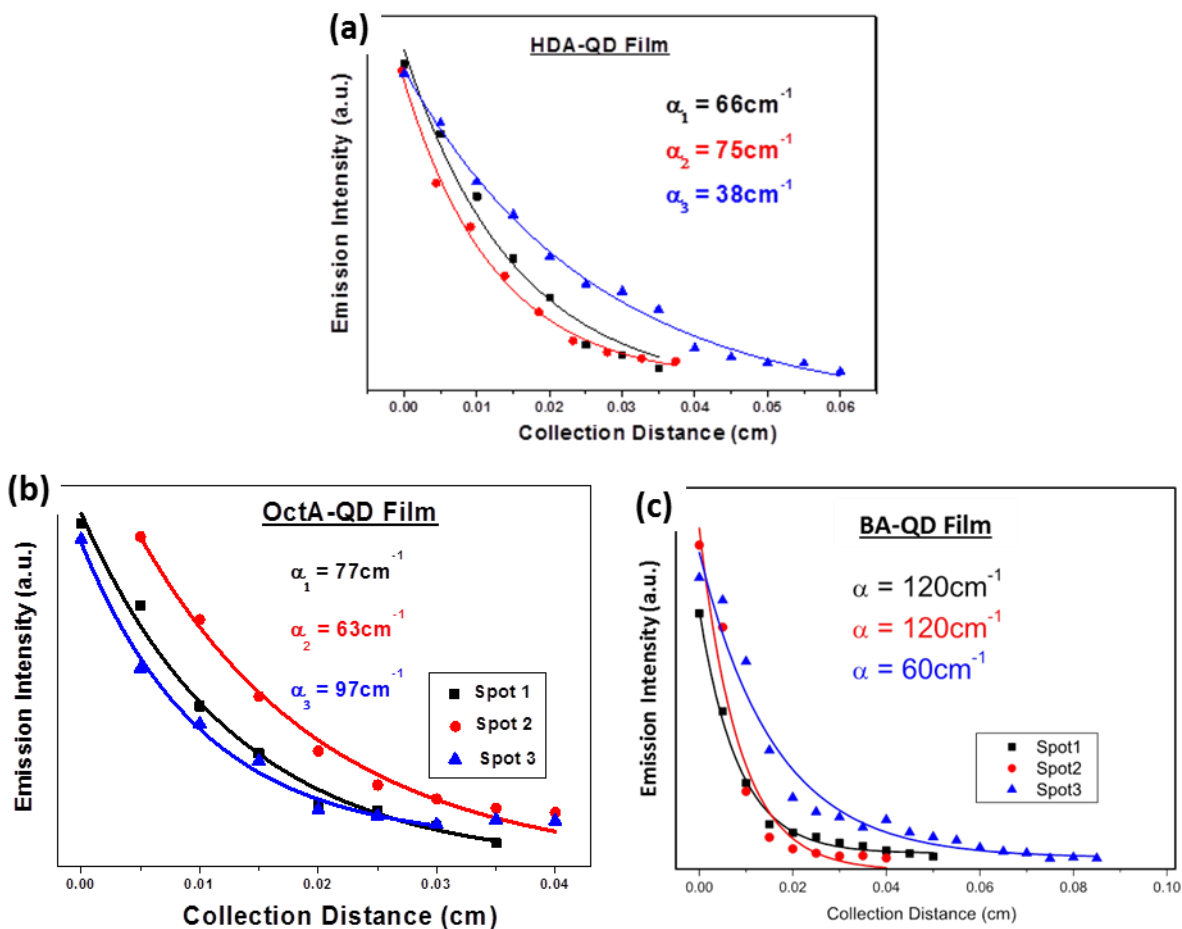


Figure S12: Plots of optical loss data and fitting for various QD-ligand combinations. The optical loss of the QD films was examined by altering the distance the emission travels through the QD film before reaching the edge of the film. The optical loss value is determined by fitting the data with an exponential decay function. The loss value for each type of QD film was determined by averaging over multiple trials. Examples of loss data and fitting are shown for (a) oleic acid-QD, (b) HDA-QD, (c) OctA-QD, and (d) BA-QD films.

Eq. S1: Equation outlining the various factors that influence the optical gain magnitude in QD films.⁶

$$G = \frac{\sigma_g \xi}{V_{dot}}$$

Where,

G = gain value

σ_g = gain cross-section

ξ = packing fraction

V_{dot} = volume of QD

Eq. S2: Equation outlining the various factors that influences the stimulated emission lifetime in QD films.⁶

$$\tau_{SE} = \frac{n_r V_{dot}}{c \sigma_g \xi}$$

Where,

τ_{SE} = Stimulated emission build up time

c = speed of light

G = gain value

n_r = effective refractive index

V_{dot} = volume of QD

ξ = packing fraction

σ_g = gain cross-section

References

- 1 Sigma-Aldrich, ChemSpider, and Chemicalize for measured and theoretical thermodynamic data and geometry data for butylamine, octylamine, hexadecylamine, oleic acid, trioctylphosphane oxide, and pyridine.
- 2 B.S. Kim, L. Avila, L.E. Brus, I.P. Herman, *Appl. Phys. Lett.* 2000, **76**, 3715-3717.
- 3 D.I. Kim, M.A. Islam, L. Avila, I.P. Herman, *J. Phys. Chem. B* 2003, **107**, 6318-6323.
- 4 S. Yakunin, L. Protesescu, F. Krieg, M.I. Bodnarchuk, G. Nedelcu, M. Humer, G. De Luca, M. Fiebig, W. Heiss, M.V. Kovalenko, *Nat. Comm.* 2015, **6**, 8056-8056.
- 5 Robert G. Hunsperger, "Integrated Optics, Theory and Technology" (DOI 10.1007/b98730). Springer New York, **2009**. Chapter 2 .Optical Waveguide Modes.
- 6 S. Hoogland, Optical gain and lasing in colloidal quantum dots, Colloidal Quantum Dot Optoelectronics and Photovoltaics. *Cambridge University Press*: **2013**.